Nina Gaiser, Hao Zhang, Thomas Bierkandt, Steffen Schmitt, Julia Zinsmeister, Trupti Kathrotia, Patrick Hemberger, Shkelqim Shaqiri, Tina Kasper, Manfred Aigner, Patrick Oßwald, Markus Köhler, Investigation of the combustion chemistry in laminar, low-pressure oxymethylene ether flames (OME0-4), Combustion and Flame 243 (2022) 122060.

The original publication is available at www.elsevier.com

https://doi.org/10.1016/j.combustflame.2022.112060

Investigation of the combustion chemistry in laminar, low-pressure oxymethylene ether flames (OME_{0-4})

Nina Gaiser[a*], Hao Zhang[a,b], Thomas Bierkandt[a], Steffen Schmitt[b], Julia Zinsmeister[a], Trupti Kathrotia[a], Patrick Hemberger[c], Shkelqim Shaqiri[d], Tina Kasper[d], Manfred Aigner[a], Patrick Oßwald[a], Markus Köhler[a]

[a] Institute of Combustion Technology, German Aerospace Center (DLR), Pfaffenwaldring 38-40, 70569 Stuttgart, Germany

[b] Department of Chemistry, Bielefeld University, Universitätsstraße 25, 33615 Bielefeld, Germany

[c] Laboratory for Synchrotron Radiation and Femtochemistry, Paul Scherrer Institute, Forschungsstrasse 111, 5232 Villigen PSI, Switzerland

[d] Mass Spectrometry in Reactive Flows, IVG, University of Duisburg-Essen, Forsthausweg 2, 47048 Duisburg, Germany

Corresponding Author*: Nina Gaiser
German Aerospace Center, Pfaffenwaldring 38-40,
70569 Stutgart, Germany
Phone: +49 -711-6862-378
Mail: nina.gaiser@dlr.de

Special Issue for Katharina Kohse-Höinghaus

Abstract

Quantitative speciation data for alternative fuels is highly desired to assess their emission potential and to develop and validate chemical kinetic models. In terms of substitute choices for fossil diesel are oxymethylene ethers (OMEs) strongly discussed. Due to the absence of carbon-carbon bonds, soot emissions from combustion of OMEs are low, but significant emissions of unregulated pollutants such as aldehydes emerge.

The combustion behavior of OME fuels with different chain lengths, OME_{0-4}, was investigated in laminar premixed low-pressure flames using complementary molecular-beam mass spectrometry (MBMS) techniques. MBMS sampling provides an *in-situ* access directly into the reaction zone of the flame. Almost all chemical species involved in the oxidation process can be detected and quantified simultaneously. Neat OME_{0-3} flames were analyzed by electron ionization (EI) MBMS with high mass resolution (R≈3900) providing exact elementary composition. To obtain isomer-specific information,

an OME_1-doped hydrogen flame and a stochiometric OME_4 flame were studied by double-imaging photoelectron photoion coincidence (i^2PEPICO) spectroscopy. Both, EI-MBMS detection and i^2PEPICO spectroscopy, enables a complete overview of all intermediates.

The results show a dominance of oxygenated intermediates for all measured conditions. Mole fraction profiles for the most important species are presented (i.e. formaldehyde, methanol, methyl formate and formic acid) and compared to modeling results. Hydrocarbons with more than four carbon atoms were not detected under the investigated conditions. Isomers such as ethanol/dimethyl ether (*m/z* = 46) and ethenol/acetaldehyde (*m/z* = 44) could be separated using threshold photoelectron spectra for clear identification and photoionization efficiency curves for quantification. This investigation permits the discussion and analysis of systematic trends, including intermediate species, for the combustion of the studied series of oxymethylene ether fuels.

Keywords: Oxygenated fuels; Oxymethylene ethers (OMEs); Polyoxymethylene dimethyl ethers (POMDMEs); Molecular-beam mass spectrometry; i^2PEPICO; Laminar flames

1. Introduction

At the recent 38th International Symposium on Combustion in 2021, Katharina Kohse-Höinghaus highlighted in her Hottel Lecture "Combustion in the Future: The Importance of Chemistry" not only the unbroken relevance of combustion, but also the importance of a deep understanding of the chemical reactions in the combustion of future fuels [1]. The ongoing transformation towards environmentally friendly energy generation is strongly coupled to process improvement and novel fuels. Especially the potential of *in-situ* chemical diagnostics and of chemical kinetics was highlighted. In this context, we are eager to present the most recent measurements performed in Bielefeld at the flame MBMS system [2-4] on a systematic series of oxymethylene ether (OME) flames.

OMEs are approved as a fuel additive for diesel engines by the European standard EN 17155 and can in principle be produced from renewable sources [5, 6]. Also known as PODEs or POMDMEs (polyoxymethylene dimethyl ethers), OMEs have the general chemical structure CH_3-O-[CH_2O-]$_n$-CH_3

with n as the number of CH_2O groups. Short-chain OMEs (OME_1 and OME_2) as well as long-chain OMEs (OME_6) are not well suited for the use in diesel engines due to low flashpoints or high melting points. Therefore, a mix of OME_{3-5} is currently discussed as the most suitable fuel for current combustion engines [5, 7]. With no direct C-C bonds present, oxymethylene ethers tend to form less soot during combustion processes [5, 6, 8].

With respect to their combustion properties, i.e., a decrease in soot emissions as well as an increase in aldehyde emissions, the combustion chemistry of oxymethylene ethers was already addressed in several studies with a special focus on OME_1 and OME_3. OME_1 was investigated in flow reactor environments by Marrodán et al. showing that the soot precursor acetylene (C_2H_2) occurs only under pyrolysis conditions [9]. Vermeire et al. have focused on developing a kinetic reaction mechanism based on the low-temperature oxidation of OME_1 in a jet-stirred reactor [10]. Jacobs et al. also presented a kinetic mechanism for OME_1 oxidation at engine-relevant conditions [11]. Sun et al. investigated OME_1 and OME_3 premixed flat flames with synchrotron vacuum ultraviolet (VUV) photoionization mass spectrometry and developed a kinetic mechanism for the combustion of these two OMEs [12, 13]. They investigated the laminar burning velocities of OME_3 flames and identified different intermediates with synchrotron VUV photoionization mass spectrometry. Following up to Sun et al., He and coworkers provided another model for OME_3 [14].. Focusing on OME_2, Ngugi et al. have studied laminar flame speed as well as ignition delay times and autoignition of OME_2 [15]. They have shown similar oxidation pathways for OME_2 and OME_1. This result was confirmed by Eckart et al. who found that OME_1 and OME_2 reach their maximum burning velocity at the same equivalence ratio of 1.2 [16]. A rapid compression machine study of OME_{2-3} shows similar ignition delay times at high pressures, while for lower pressures the ignition delay times differ noticeably [17]. Cai et al. have recently demonstrated in shock tube experiments that the impact on fuel reactivity vanishes at high pressures with increasing length of the OME. They developed a kinetic model up to OME_4 [18]. A reduced OME_n mechanism for engine applications was developed and validated up to OME_3 by Ren et al. [19]. Very recently, Kathrotia et al. have published a new model primarily focused on various hydrocarbon classes but also includes higher oxymethylene ethers from OME_0 (dimethyl ether) up to OME_5 [20-22].

In this work, a systematic investigation of the combustion chemistry for a series of oxymethylene ethers is presented to improve the understanding of the influence and effects of different chain lengths. To this end, the combustion behavior of the fuels OME_{0-3} was investigated in laminar premixed low-pressure flames using complementary molecular-beam mass spectrometry (MBMS) techniques at identical conditions. MBMS sampling provides an *in-situ* access directly into the reaction zone of the flame. Almost all chemical species involved in the oxidation process can be detected and quantified simultaneously, including highly reactive species such as radicals. Neat OME_{0-3} flames were analyzed by electron ionization molecular-beam mass spectrometry (EI-MBMS) with high mass resolution ($R \approx 3900$) at Bielefeld University, providing the exact elementary composition of the involved species. Special emphasis was given here to the identification and occurrence of intermediates and their mole fraction tendencies in relation to the chain length of the fuel. The resulting quantitative mole fractions are provided as a function of the height above the burner (HAB).

Subsequent in-depth identification of combustion intermediates [23, 24] with separation of isomers was performed at the i^{2}PEPICO endstation (X04DB) at the Swiss Light Source (SLS) using tunable synchrotron VUV photoionization mass spectrometry. Two flat premixed flames, one fuel-rich OME_1-doped hydrogen and one stoichiometric OME_4 flame, were investigated and used for the identification of isomeric intermediates. The results are complemented with the flame modeling using the DLR reaction mechanism [20].

2. Experiment

Two different experimental flame setups were used for a detailed systematic investigation of the series of oxymethylene ethers: the EI-MBMS flame setup at Bielefeld University [3, 25, 26] and the i^{2}PEPICO endstation [27-29] at SLS in Villigen, Switzerland. Both are described elsewhere, so only a brief description is given here. DME, i.e., OME_0 (>99.9 % purity), was purchased from Linde and OME_1, also known as methylal or dimethoxymethane, from Sigma-Aldrich (>99 % purity). All larger OMEs were purchased from ASG Analytik-Service and had a purity of ~98 %. Small amounts of OMEs with different chain lengths account for the remaining 2 %.

2.1 EI-MBMS

For each OME_n (n=0-3), a fuel-rich, premixed laminar flame was investigated using the EI-MBMS setup to get an overview into the oxidation behavior of OMEs. Flame conditions are summarized in Table 1.

Table 1: Experimental flow conditions (slm at 273 K; 1013 mbar) of the investigated laminar flames (EI-MBMS). T_{ad}: adiabatic flame temperature [20, 30]

	Fuel	O_2	Ar	ϕ	T_{ad} / K	p / mbar
 OME_0	0.686 slm x_{Fuel}=0.18	1.21 slm x_{O2}=0.32	1.9 slm x_{Ar}=0.5	1.7	2456	40
 OME_1	0.566 slm x_{Fuel}=0.15	1.33 slm x_{O2}=0.35	1.9 slm x_{Ar}=0.5	1.7	2453	40
 OME_2	0.482 slm x_{Fuel}=0.13	1.42 slm x_{O2}=0.37	1.9 slm x_{Ar}=0.5	1.7	2452	40
 OME_3	0.419 slm x_{Fuel}=0.11	1.48 slm x_{O2}=0.39	1.9 slm x_{Ar}=0.5	1.7	2451	40

The experimental setup consists of a vertically moveable homemade flat-flame bronze burner (Ø = 63.82 mm) which is water-cooled to a temperature of 333 K. Flows of argon, oxygen and dimethyl ether were controlled and metered by Coriolis flow meters (Bronkhorst, Mini Cori-Flow M14, M13, M12 and ML-120/±0.5 % precision) to ensure a precise flow rate and mixture composition. Liquid fuels were evaporated in a standard vaporizer system (Bronkhorst/Controlled Evaporation Mixing - CEM) with argon as the carrier gas. This standard vaporizer systems provides constant evaporation combined with a highly sensitive monitoring system to ensure a complete evaporation of the used fuel. The operation of the Bronkhorst CEM follows the principle: liquid fuel is drawn from a pressurized syringe pump (Harvard Apparatus) and is measured by a liquid Coriolis mass flow meter (±0.2 % precision). Then, the liquid fuel enters the Bronkhorst CEM mixing chamber controlled to a setpoint value by a control valve. The formed mixture is subsequently led into the evaporator to achieve full evaporation [31]. The temperature of the vaporizer was set to 423.15 K for OME_3 and 323.15 K for OME_2 at a pressure of 2 bar absolute. All gases were fed over heating hoses (4 mm inner diameter) to prevent condensation and were mixed before entering the burner. The flames were stabilized at a pressure of 40 mbar with a total inlet flow rate of 3.8 slm, an environment that widens the reaction zone of the flame. A quartz

nozzle (~500 µm orifice) was used to withdraw gas samples at different flame positions (height above burner (HAB), 0-30 mm) with a spatial resolution of 0.25 - 0.5 mm. Rapid expansion of the sampled gas into high vacuum (10^{-4} mbar) forms a molecular beam, which is guided through a copper skimmer into the ionization chamber of the mass spectrometer (10^{-6} mbar). A two-stage Wiley-McLaren ion source coupled to a reflectron time-of-flight (TOF) detection unit with a mass resolution R ≈ 3900 is suitable to resolve exact elemental composition (C/H/O) in this system. The ionization energy was set to 15 eV for major species detection, while 10.5 eV and 12 eV were used for intermediate species detection to minimize fragmentation.

Note that the experimental data for OME_1 and DME shown here are also discussed by Zhang et al. to evaluate their potential as reaction enhancers for methane in polygeneration processes [32].

2.2 i²PEPICO

Using the i²PEPICO instrument, a laminar premixed OME_1/hydrogen flame and a neat OME_4 flame were investigated. Flow conditions are displayed in Table 2.

A McKenna-type flat-flame burner (Ø=60 mm) was used for stabilization of the premixed laminar flames. Liquids were evaporated and were with all other gases transferred to the flame as in the EI-MBMS setup. Evaporation follows the same principle as with EI-MBMS. Gas samples, as a function of the height above the burner (spatial resolution of 0.25 - 0.5 mm), were withdrawn from the flame with a quartz nozzle (210 µm opening), expanded through the first pumping stage (10^{-5} mbar) and through a copper skimmer into the ionization chamber (10^{-6} mbar). Synchrotron VUV radiation within the range of 6–16.2 eV provided soft photoionization. The i²PEPICO spectrometer enables coincident detection of electrons and ions formed during the ionization process. This technique allows isomer-selective species identification and quantification [29] thanks to the measurement of both mass-selected threshold photoelectron spectra (ms-TPES) and photoionization efficiency (PIE) curves [33].

Table 2: Experimental flow conditions of the investigated laminar flames (i²PEPICO).

		Fuel	H_2	O_2	Ar	ϕ	p / mbar
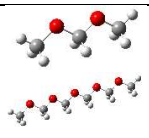	OME_1/H_2	0.20 slm x_{Fuel}=0.05	1.8 X_{H2}=0.45	1.0 slm x_{O2}=0.25	1.0 x_{Ar}=0.25	1.7	40
	OME_4	0.25 slm x_{Fuel}=0.0625	-	1.75 slm x_{Fuel}=0.4375	2.0 slm x_{Fuel}=0.5	1.0	30

2.3 Data evaluation and uncertainties

Mass spectrometric investigations of OMEs with EI-MBMS and photoionization (PI) are complicated by the fact that all OMEs, except for DME, do not form stable molecular ions upon ionization [12, 34] and instantaneously fragment towards smaller ions. For EI-MBMS, a fragment is used for the evaluation of the fuel signal: the molecular $C_2H_6O^+$ ion is chosen for DME, $C_3H_7O_2$ for OME_1 and $C_4H_9O_3$ for all higher OMEs. In photoionization cold gas measurements, an ionization energy of 9.75 eV could be determined for OME_4. The observed fragmentation pattern is shown in Fig. 1. Even though soft ionization is provided through the synchrotron VUV light source, OME_4 shows a variety of fragments. However, fuel fragmentation was corrected properly, but precludes a direct measurement of the fuel radicals with i²PEPICO [29].

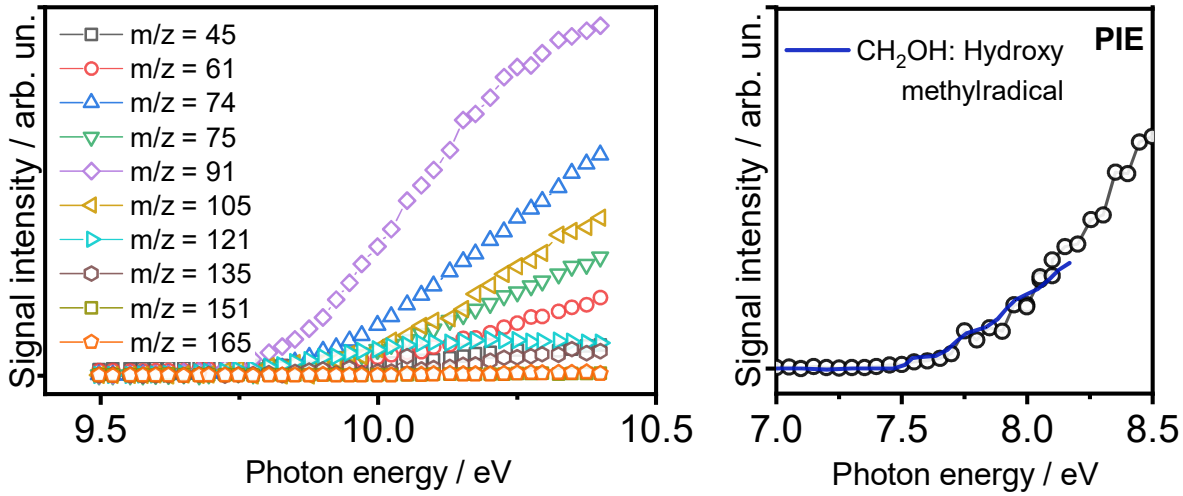

Fig. 1: Cold gas photoionization efficiency spectrum of OME_4 (m/z= 166) fragments (left), no stable parent ion is formed. Simulated PIE spectrum (blue line) of hydroxyl methyl [35] compared to experimental PIE curve at m/z = 31 (right).

Data evaluation followed the established procedures described in [26] for EI-MBMS and in [27, 29, 36] and i²PEPICO, respectively. The integrated and corrected ion signals were connected to their mole fractions (x_i) by comparison to the respective signal of the inert gas argon. For EI-MBMS, corrections for background and fragmentation of species through the ionization process were performed with

consideration of fragmentation patterns of the directly calibrated species. Additionally, raw signals were corrected for ^{13}C and ^{18}O isotopes where necessary. Mole fractions of major species were calculated from direct calibration with CO/CO_2 mixtures and internal calibration by element balances of C, H, and O. Labile species (EI-MBMS) were not directly calibrated, but quantified by the relative ionization cross section (RICS) method [37] or the convolution of the literature ionization cross sections with the known energy distribution of the electrons [3]. Species using direct calibration, uncertainty ranges up to 30 %, while for other species that could not be calibrated directly, the uncertainty increases to a factor of 2-4 [32]. Experimental uncertainties are given as "Error" in the corresponding graphs for each species instead of error bars to ensure the readability of all figures.

The i^{2}PEPICO measurements focus on intermediate detection and isomer separation primarily to confirm the identity of different OME_n oxidation intermediates. For the first time, samples of an OME_4 flame were examined. The SLS flame setup allows isomer-selective species identification using i^{2}PEPICO spectroscopy, but due to the low mass resolution isobaric species may be convoluted, too. Therefore, the results of i^{2}PEPICO focus on characteristic mass-to-charge ratios (m/z) for OME flames and identify several intermediates on the basis of their photoionization efficiency (PIE) curves as well as their threshold photoelectron spectra (TPES). Radicals can be detected at positions in the flame, where the overlap with fuel fragments is low enough as shown in Fig. 1 for the example of $m/z = 31$. Using the photoionization curve for photon energies between 7 and 8.5 eV, the hydroxymethyl radical (CH_2OH) is clearly identified. This radical plays an important role in the decomposition of OME as direct sources of formaldehyde [38]. The clear identification of important isomers by i^{2}PEPICO supports the legitimacy of the quantification of the EI-MBMS results and provides additional information for validation and improvement of kinetic models. Furthermore, the analysis of the photoionization data is used to validate the calibration factors applied in the evaluation of the EI-MBMS data.

2.4 Flame temperature

Flame temperature profiles were obtained following the sample-rate based procedure described by Struckmeier et al. [4] or Krüger et al. [39], using the exhaust gas temperature as well as the pressure in the first pumping or ionization stage. Introducing a sampling nozzle disturbs the flame primarily by

cooling the flame temperature [39-43], but for small distances between burner and sampling nozzle, other effects have to be considered [44]. Depending on the actual temperature, the sampling rate, i.e., the amount of gas flowing through the orifice, is changing and the relative changes can be obtained from the pressure change in the first pumping or ionization stage. Relations between pressure and flame temperature can be found in [4, 29, 45]. Exhaust gas temperatures were measured at HAB = 25 mm by using a type R thermocouple by OMEGA (Ø = 0.45 mm) coated with SiO_2 (silicon dioxide). The temperature measurements have been performed in the same apparatus after the relocation to Stuttgart. No sampling nozzle was installed while obtaining temperature profiles. Radiation correction was performed following previously reported procedures [32, 46], based on a reference DME flame (ϕ = 1.7 / measured at Bielefeld University) [32, 47] temperature measured by OH planar laser-induced fluorescence (PLIF) [48]. The uncertainty within the temperature measurements is estimated to be ±10 % [48]. All temperature profiles can be found in the Supplemental Material I. The exhaust gas temperatures for all OME flames are very close to each other in the range of 2000 K.

3. Results and discussion

Interpretation of the results is supported by modeling of the flames using the DLR reaction mechanism of Kathrotia et al. [20], which is currently the only available model that includes all OMEs from DME up to OME_5. Simulations were performed using open-source Cantera [49] and the Cantera flame reactor module for burner-stabilized flames within the Chemical Workbench [50]. The temperature profiles, as shown in Fig. 2, were used as input for the flame calculations. Respective results are compared to the experimental findings, whereby good agreement is generally found.

3.1 Main species

Figure 2 shows the experimental and numerical data for the main species and temperature profiles for all investigated fuel-rich OME_n (ϕ = 1.7) flames. The comparison shows that trends for the main species are excellent in line with the kinetical model [20], which are represented as solid lines.

Focusing on the fuel consumption, it can be seen that OMEs with longer chain lengths (n = 2-3) are consumed faster, i.e., complete consumption is observed closer to the burner surface compared to DME

and OME_1. As a consequence, the position of the reaction zone is moving to larger distances with decreasing chain length [51]. Indeed, the laminar flame speed is found to increase with the OME chain length [15, 16, 52, 53]. This is even more obvious when the CH_2O peak maxima, one of the first species formed (see Fig. 3), are compared. Furthermore, for the larger OMEs the proximity of the reaction zone leads to be increased in the gas phase near the burner surface. This is also in line with the ignition delay-time behaviour of the OMEs: the ignition delay times of OMEs are getting shorter with the length of the OME [54]. Longer OMEs are therefore decompose at lower temperatures and therefore closer to the burner surface. A comparable behavior for long-chain OMEs was observed in atmospheric laminar flow reactor experiments demonstrating that shorter chain lengths correlates with higher temperatures [55] needed for total oxidation. This finding is in line with the cetane numbers (CN) of OME_{1-3}, which increase from 26 for OME_1 up to 78 for OME_3 [56]. High cetane numbers correlate with lower autoignition temperatures. In both cases the difference becomes smaller with increasing chain length, i.e., is most prominent between OME_0 and OME_1 and vanishes for the largest pairs.

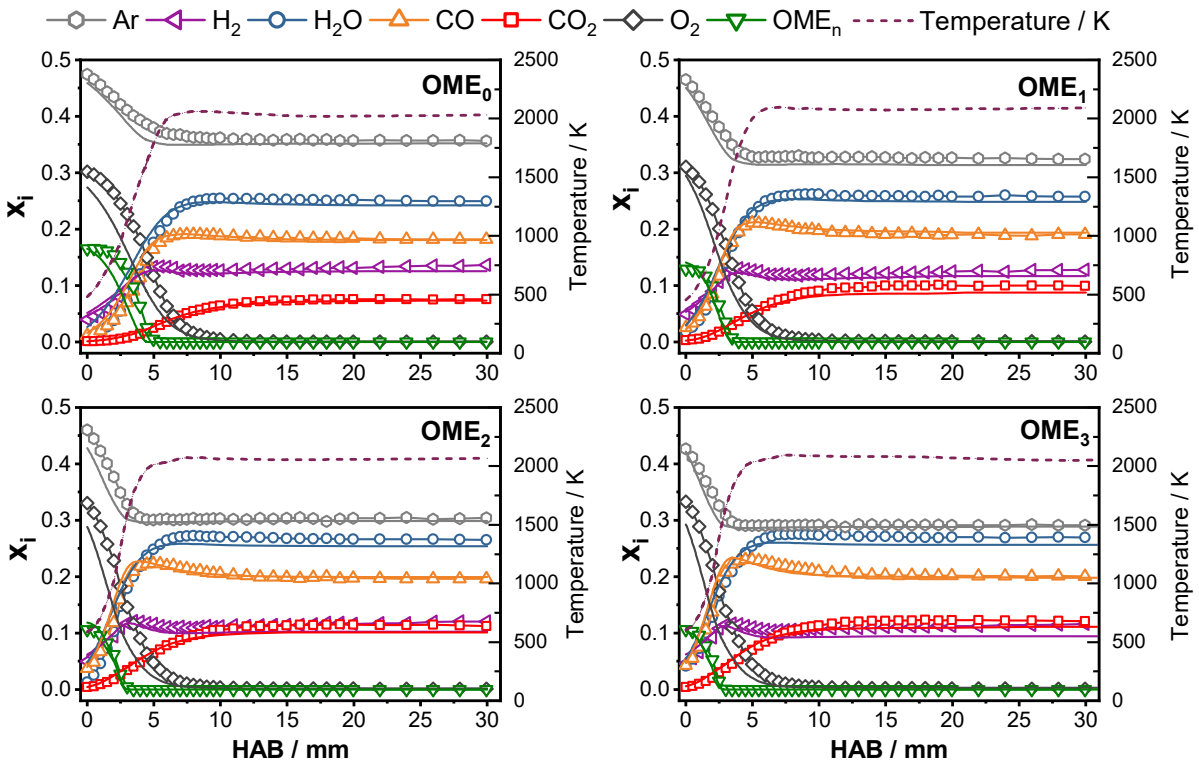

Fig. 2: Main species mole fraction profiles (dots) and temperature profiles (dashed lines) of OME_{0-3} flames using EI-MBMS compared to model predictions (solid lines) [20].

3.2 Oxygenated intermediates

Due to the lack of C-C bonds, oxygenated species are the dominant intermediates for all investigated OMEs. The obtained species pool is thereby quite similar for all OMEs. Small oxygenated species, which are relevant for the combustion process of OME_1, also play an important role for all higher OMEs. Fig. 3 shows the mole fraction profiles of formaldehyde and methanol. Formaldehyde turns out to be the main intermediate with the highest mole fraction for all investigated fuels, followed by methanol and methyl formate for OME_{1-3}. Note that the mole fraction profile of methyl formate is given in Fig. 7. The model shows a good prediction for formaldehyde in position, trend between the OMEs, and absolute mole fraction. Formaldehyde profiles, as one of the first intermediate, reflect the shift in the reaction zone due to increasing flame speeds with the OME chain length.

All OMEs decompose primarily by the abstraction of a terminal H since the bond dissociation energy of the C-H in the $-OCH_3$ moieties is smaller than in the $-OCH_2O-$ moieties [12]. A detailed reaction path analysis for OME_{1-3} based on the DLR mechanism [20] is provided within Supplemental Material II.

For example, OME_3 decomposes by 90.6 % via its primary radical $CH_2OCH_2OCH_2OCH_2OCH_3$, while for both secondary radicals the remaining shares are divided equally (see Fig. S 1). Further decomposition leads to CH_2O and the primary radical of the next smaller $OME_{(n-1)}$. This sequence of consecutive β-scissions is repeated down to the smallest unit (methoxy methyl radial) CH_2OCH_3 that itself decompose to methyl and formaldehyde. Consequently, the amount of formaldehyde detected in the flames (Fig 3) is increasing systematically with increasing OME chain length.

Methanol predictions are less convincing and mole fractions are underpredicted roughly by a factor of 10 (except for DME). The similarity of profiles for OME_{1-3} is also not well predicted. Methanol is likely a product of thermal decomposition of methyl formate [6] and the trends in the formation of methyl formate are not predicted very well (see section 3.6 and discussion of m/z = 60 (Fig. 7)).

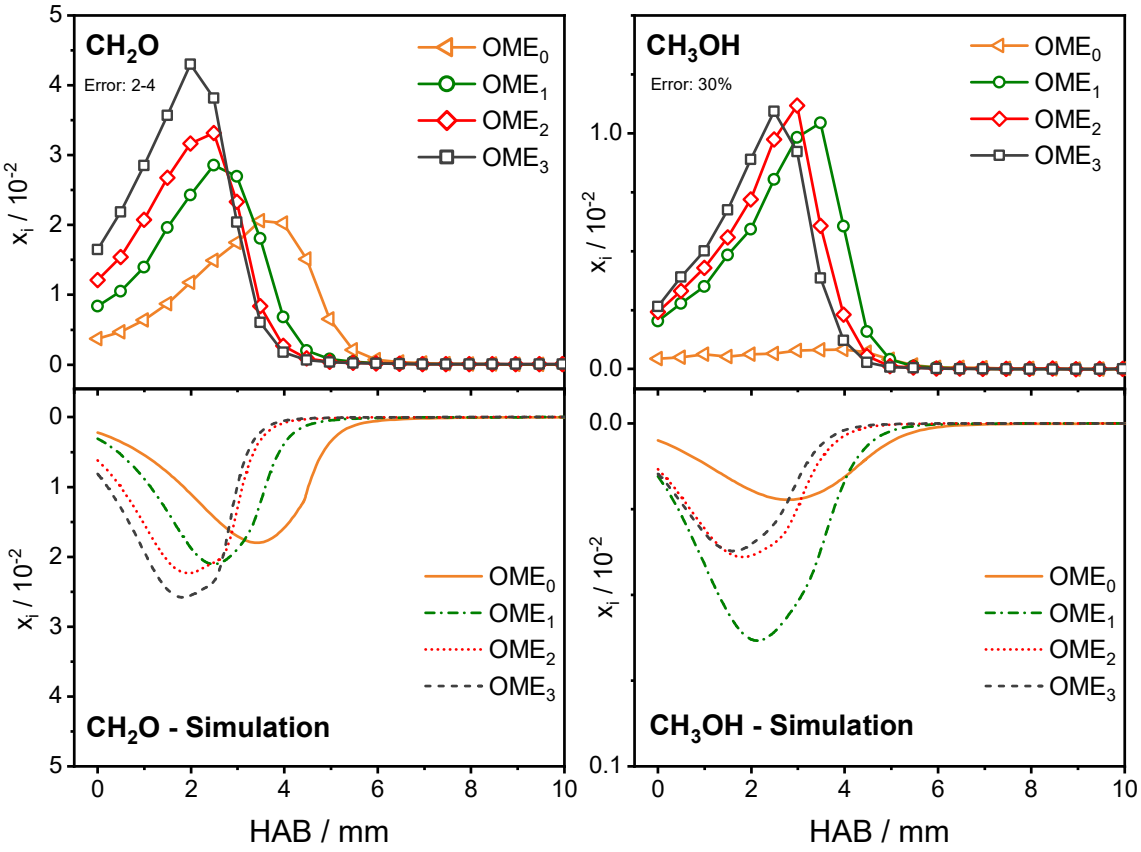

Fig. 3: Mole fractions profiles of formaldehyde (CH_2O) and methanol (CH_3OH) for all investigated OME_{0-3} flames using EI-MBMS (upper panels) conditions (ϕ = 1.7) compared to model prediction (lower panels). Note deviating x_i-axis for methanol.

3.3 Species with C-C bonds

Even though OMEs do not have direct C-C bonds, several C_2-C_4-hydrocarbons were detected in the combustion process of OMEs, namely C_2H_2, C_2H_4, C_3H_4, C_3H_6, C_3H_8, C_4H_4 and C_4H_6 (Fig. 4 and Supplemental Material I). In the complete flame series, the species with the longest carbon chain detected are butadiene and vinylacetylene. Note, that mole fractions of the C_4 species are close to the detection limit (~ $4\text{-}8 \cdot 10^{-6}$) and are reasonably predicted by the model. Profiles can be found within Supplemental Material I.

Main formation pathways for all species with C-C bonds are – because of the lack of C-C bonds in the fuel – the initial recombination reactions of the intermediately formed CH_3 radicals [57, 58]. In general, the model prediction of the hydrocarbon species pool is good. The majority of hydrocarbon intermediates is predicted within the experimental uncertainty limits. However, some model predictions

deviate for some C_3 species (e.g., C_3H_6 and C_3H_8). Regarding the methyl profile, there is a discrepancy between the model and the experimental data: for OME_0 the experimental data show a lower maximum mole fraction compared to the one of OME_1, while in the simulations the maximum mole fraction of OME_0 is the one with the biggest maximum. Similar trends can be seen for C_2H_4, C_2H_6, C_3H_6. Note that absolute concentrations of those intermediates are two orders of magnitude lower than the C_2-hydocarbons.

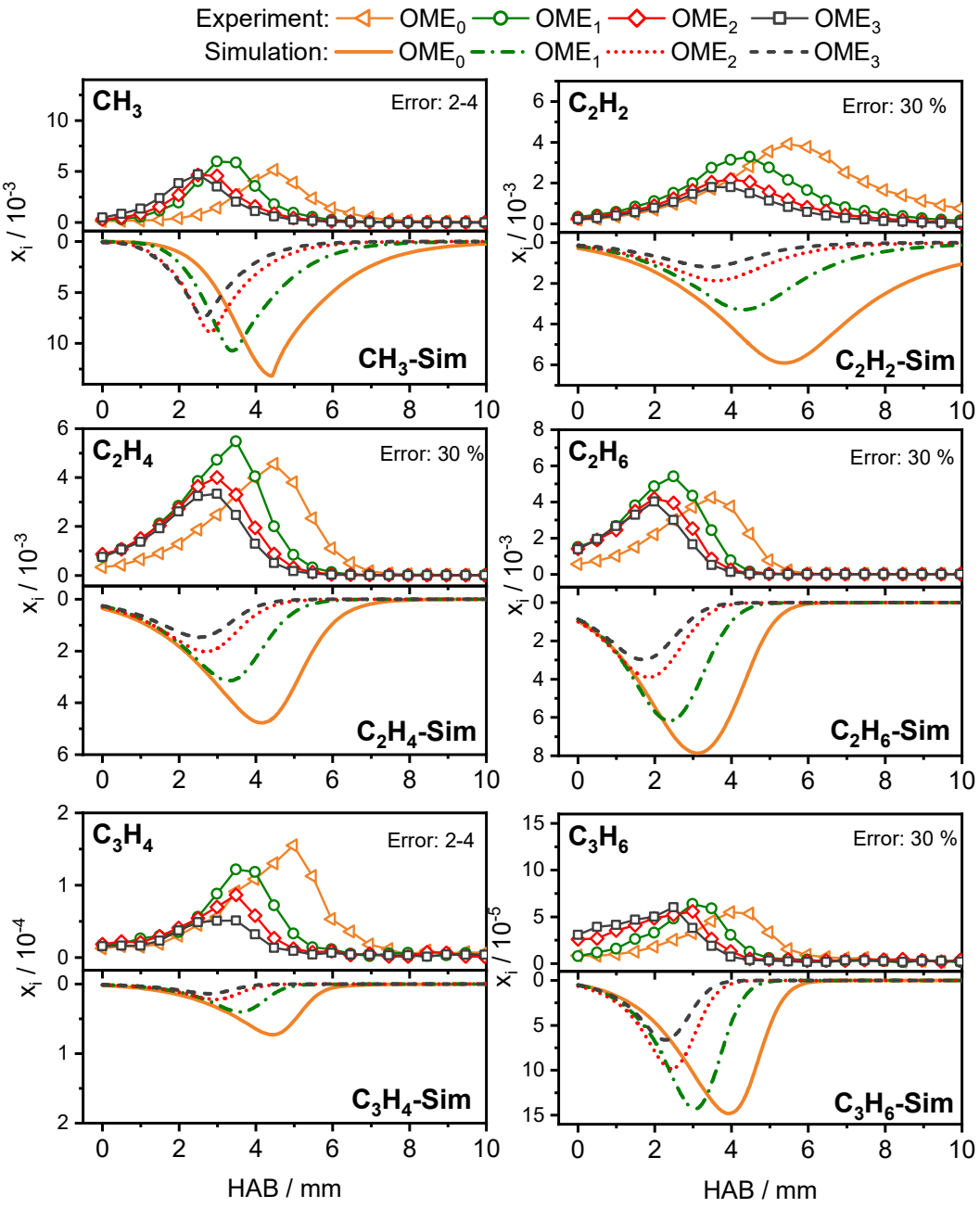

Fig. 4: Experimental (EI-MBMS) mole fraction profiles of hydrocarbon intermediates (upper panels) in comparison to simulation for $OME_{0\text{-}3}$ flames (lower panels).

3.4 Identification of species with *m/z* = 44

Figure 5 provides ms-TPES, PIE curves and mole fraction profiles of the species detected at *m*/*z* = 44. PIE curves of *m*/*z* = 44 for the OME_4 flames indicate the presence of ionization thresholds of the C_2H_4O isomers ethenol and acetaldehyde. Both isomers are identified in the measured PIE curve by comparison with the weighted sum of individual photoionization cross sections and are common intermediates in hydrocarbon flames [59]. The PIE curve additionally suggests the presence of a third C_2H_4O isomer: ethylene oxide. Furthermore, the strong increase of the PIE curve at 10.9 eV indicates the presence of propane, C_3H_8, which can be confirmed by its exact mass in the OME_{0-3} flames by EI-MBMS. Apparently, the identification and separation of multiple isomers and isobars is difficult since specific features of the PIE curves, i.e., distinctive steps at the ionization threshold, are vanishing with increasing number of isomers. This ambiguity is withdrawn by the observation of the TPES, where all species exhibit individual spectral peaks and the presence of all above mentioned species is confirmed for the OME_1/H_2 flame. In particular the presence of ethylene oxide is consistent with results of Kasper et al. from PIE curves measured in a tetrahydrofuran flame [60]. They assume stabilization of $(CH_2)_2O$ to the cyclic ethylene oxide to be a viable reaction even at high temperatures.

Quantitative species profiles given in Fig. 5 are obtained from the EI-MBMS and thus the C_2H_4O isomers are not separated. The combined signal was calibrated according to the main isomer acetaldehyde. Despite the increased experimental error caused by the rough calibration prediction, the prediction of the DLR model is still reasonable for the sum of C_2H_4O isomers.

Propane, in contrast, is the only possible C_3H_8 isomer and its experimental uncertainty is on the order of factor 2 due to application of the RICS calibration. Compared to the model by Kathrotia et al., for all OMEs, propane is overestimated clearly beyond the experimental uncertainty (approximately a factor 10) for all OMEs.

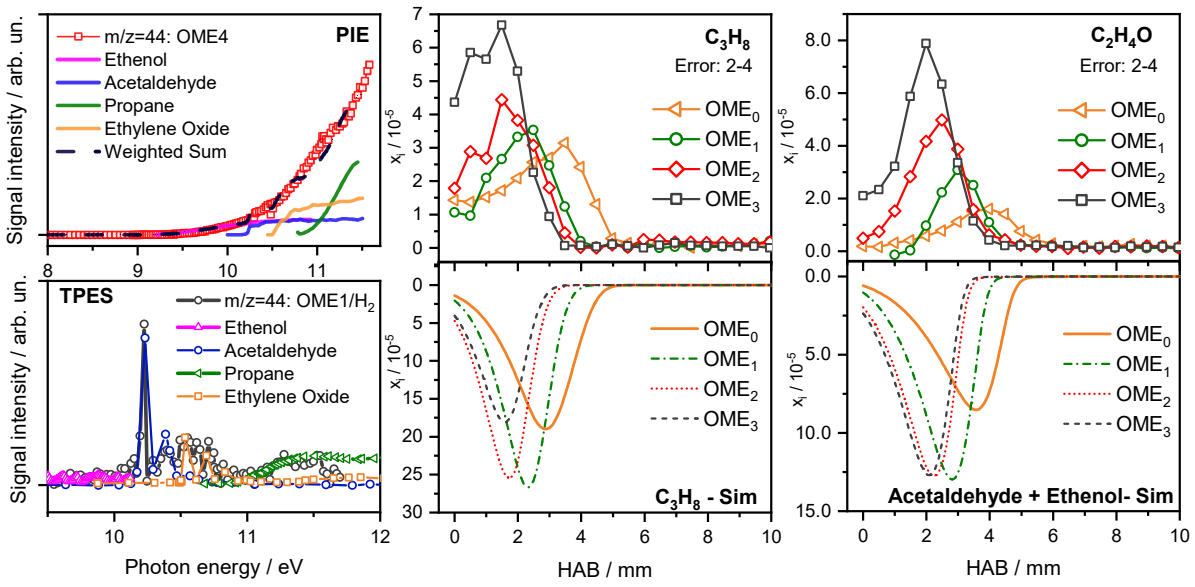

Fig. 5: Photoionization efficiency (PIE) curves and threshold photoelectron spectra (TPES) of $m/z = 44$ for OME_1/H_2 and OME_4 flames in comparison with literature spectra [60-63] (left column). Experimental EI-MBMS mole fraction profiles (upper panels) in comparison to simulation for OME_{0-3} flames (lower panels) for C_3H_8 (middle column) and all C_2H_4O isomers (right column). Note deviating x_i-axis (experiment/model).

3.5 Identification of species with $m/z = 46$

Figure 6 shows the photoionization efficiency curves (PIE) as well as the threshold photoelectron spectra (TPES) of $m/z = 46$ and compares the measured PIE curve to the weighted sum of respective literature photoionization cross sections. The analysis ascertains the presence of dimethyl ether, formic acid and ethanol in the OME_4 flame, while only minor ethanol concentrations beside formic acid and dimethyl ether can be proven in the OME_1/H_2 flame. Traces of dioxirane can also be observed from the best fit of the weighted sum of cross sections to the PIE curve. Dioxirane, a three-membered ring species with an O-O bond is a stable species, but tends to be a short-lived intermediate at combustion-like conditions [64, 65]. Due to the short lifetime, the detection of dioxirane is challenging in the flame experiment. No clear conclusion can be drawn here, whether dioxirane is present or not. However, dioxirane is neither included in the DLR mechanism nor in any other OME mechanism [11, 12, 14, 18-20]. Furthermore, DME is available in a higher ratio for the OME_1/H_2 compared to the neat OME_4 flame. For the neat OME_4, the best fit shows a ratio of 66 % ethanol to 33 % DME. Having a higher mole fraction for

ethanol compared to DME was already observed in atmospheric, laminar reactor measurements for pure $OME_{1\text{-}5}$ [55]. For the OME_1/H_2, the ratio of DME account for 98 % compared to ethanol. The higher mole fraction of DME compared to ethanol is also underlined by the strong fraction of DME in the TPES, seen in Fig. 6. [55]. This is likely due to the increased importance of the formation route $CH_3OCH_2 + H_2 = CH_3OCH_3 + H$ at the H_2 rich base flame. For the neat OME flames, most CH_3OCH_2 is directly decomposed to formaldehyde [12]. Comparing the sum of C_2H_6O isomers from EI-MBMS measurements to the modeling results of ethanol and DME, it can be seen that the model also provides a higher mole fraction of ethanol compared to DME, but in a ratio of ~100:1. Comparing the overall mole fraction is challenging due to the fact that C_2H_6O is completely calibrated as DME for the EI-MBMS results. Calibrating *m/z= 46* as a combination of DME and ethanol for $OME_{0\text{-}4}$, the overall mole fraction is even increasing. Since we do not have measured the isomer ratios for $OME_{0\text{-}3}$, the current provided data is not sufficient to draw any further conclusions at this point. More isomer-selective research has to be conducted in this area.

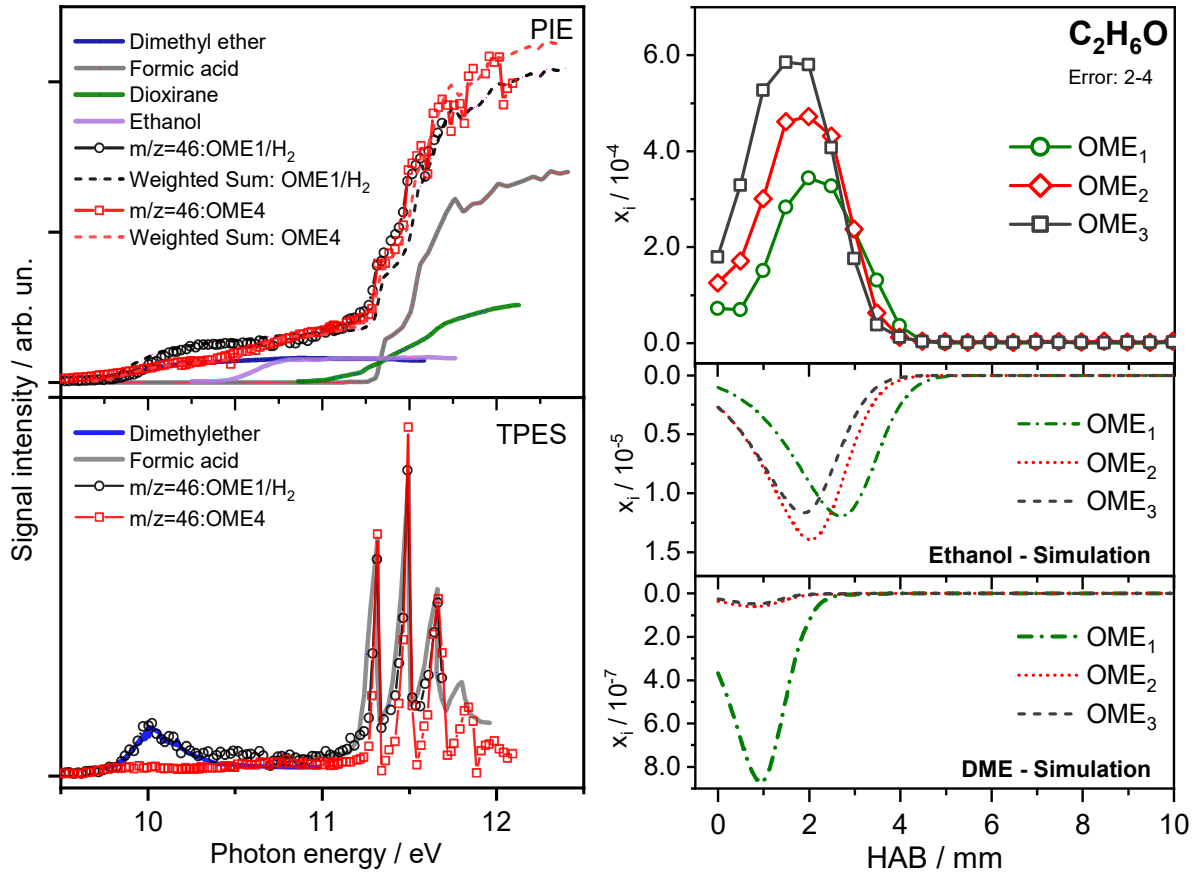

Fig. 6: Photoionization efficiency (PIE) curve and threshold photoelectron spectra (TPES) of *m/z* = 46 for OME_1/H_2 and OME_4 flames in comparison with literature spectra [63, 66-69] (left). Mole fraction profiles (right) of C_2H_6O (sum of isomers) for the investigated OME_{1-3} flames using EI-MBMS compared to model predictions of intermediate ethanol and DME. Evaluation of the *m/z = 46* signal in OME_0 fail due to strong interference with the fuel.

3.6 Identification of species with *m/z* = 60

The PIE curve in Fig. 7 indicates the presence of vinyl hydroperoxide by comparison to the calculated PIE spectrum by Taatjes et al. [70]. Hydroperoxides are typical low-temperature oxidation products. Bierkandt et al. have already shown that these low-temperature species are formed very close to the burner surface in laminar low-pressure flames [40]. Furthermore, Zhang et al. have also detected low-temperature intermediates like hydroperoxides by flame-sampling molecular-beam mass spectrometry [41].

For both flames investigated by i^2PEPICO, methyl formate was identified by its TPES and detected in the OME_{1-3} flames; its maximum mole fraction decreases slightly from $1.1 \cdot 10^{-2}$ for OME_1 to $8.4 \cdot 10^{-3}$ for OME_3. The model prediction for OME_1 and OME_0 agrees well with the measurement while the slight decrease for larger OMEs is not reproduced well. The model rather predicts a similar but significantly lower mole fraction for OME_2 and OME_3. For higher OMEs, methyl formate is a product of thermal decomposition [6]. Methanol (see Fig. 3), as reported by Peukert et al. [2] for OME_1, is primarily formed from methyl formate during subsequent thermal decomposition steps. Since methanol and methyl formate peak at similar HABs in similar concentrations for OME_{1-3}, similar reaction pathways can be assumed for all higher OMEs. The same trend was observed in atmospheric reactor measurements [55]. This formation pathway can be underlined by the fact that no methyl formate is formed in the pure DME flame, but in those of all higher OMEs (Fig. 7).

Yu et al. have found another formation pathway for methanol in thermal decomposition of OME_1 [71]: They suggest that a hydrogen migration and subsequent methanol loss yields methoxymethylene carbenes (CH_3-O-CH), which are thermodynamically favored over the direct C-H and R-O bond scission. Carbenes are very short-lived intermediates especially at elevated temperatures, where they

directly decompose. Currently, no methoxymethylene carbenes were detected neither in the pyrolysis nor in the flame measurements. Because of the similar decomposition behavior of all OMEs, it can be assumed that the methanol formation route is applicable for all higher OMEs likewise.

An isobaric species at $m/z = 60$ is methoxyethane (C_3H_8O). Its formation is confirmed in both flames by comparison of the measured ms-TPES (i^{2}PEPICO) with the spectrum of literature data (see Fig. 7) as well as by its exact mass determined in the EI-MBMS. In previous atmospheric reactor measurements, C_3H_8O was only detectable in very small amounts during OME_{3-5} oxidation [55]. Methoxyethane is currently not integrated in any of the available mechanisms [11, 12, 14, 18-20], and its addition to the kinetic reaction scheme may improve the prediction quality of the current models for OME combustion. The formation of methoxyethane was also observed in DME flames by Cool et al. [72], with the most abundant formation way *via* $CH_3OCH_2+CH_3 = CH_3OCH_2CH_3$. Methoxyethane can decompose into methanol and ethylene as discussed by Yasunaga et al. [73]. No evidence was found for the presence of CH_3CHOO, having a photoionization energy of 9.3-9.4 eV [70], 1,2-dioxetane, or propanol.

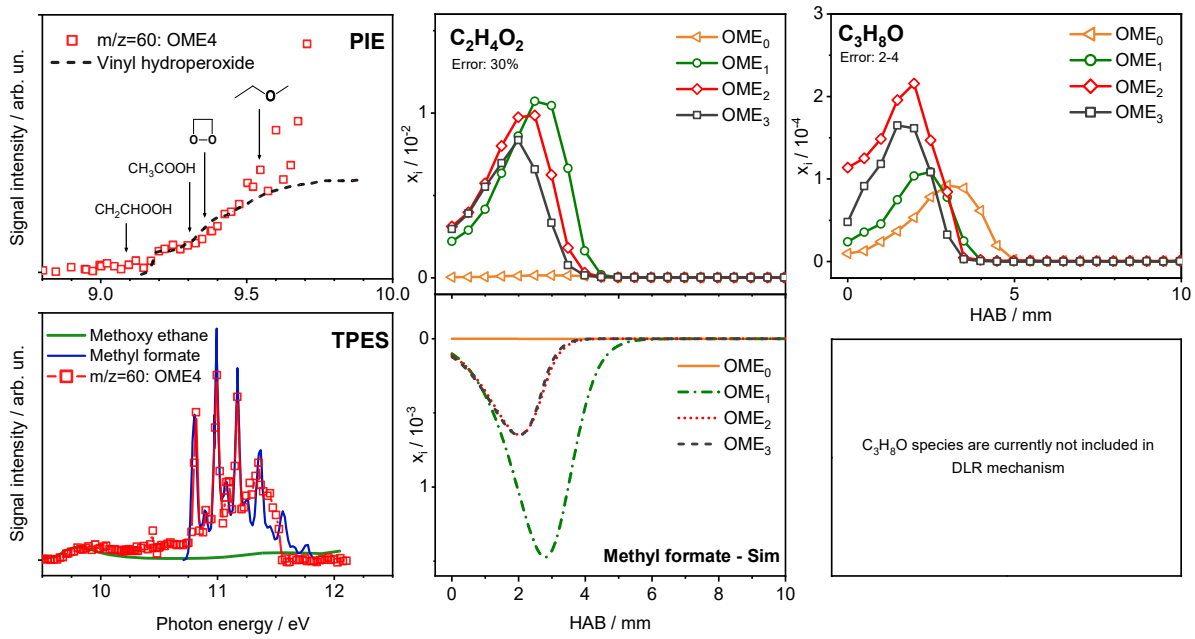

Fig. 7: Photoionization efficiency (PIE) curve and threshold photoelectron spectra (TPES) of $m/z = 60$ for the OME_1/H_2 and OME_4 flames in comparison with literature spectra [69, 70, 74] (left). Mole fraction profiles of C_3H_8O (quantified as methoxy ethane) and $C_2H_4O_2$ (quantified as methyl formate) for the investigated OME_{0-3} flames (right) using EI-MBMS compared to model results.

4. Conclusion

This study presents a systematic investigation of the oxidation behavior of oxymethylene ethers with different chain lengths (n = 0,1,2,3,4). Dimethyl ether (DME) is indexed as OME_0. Two different experimental setups were used to gain information about the combustion process and details of isomerization of intermediates formed in the combustion of longer-chain OMEs. Isomer-selective intermediate identification was successfully performed at the i^2PEPICO flame setup in a fuel-rich OME_1-doped hydrogen flame and in a stoichiometric OME_4 flame. Furthermore, fuel-rich OME_{0-3} flames (ϕ = 1.7) were investigated by EI-MBMS. Systematic speciation for flames on the consecutive series is presented and available with the electronic supplement.

All measured oxymethylene ethers do not form stable cations upon photoionization and instantaneously fragment towards smaller ions. For all OMEs, oxygenated species are the dominating intermediates in the combustion process with formaldehyde showing the highest mole fractions. Higher oxygenated combustion intermediates are methoxyethane and methyl formate. No typical soot precursors were detected even for the fuel-rich conditions. The systematic investigation confirms increased reactivity for higher OMEs, detected by a shift of the burner position of typical intermediates and therefore a shift in peak temperature to lower temperatures. The observed species pool is nearly independent of the chain length of the respective OME. Experimental findings are compared to the present comprehensive DLR model [20] presently the only available model for OME_{0-5}. All key features of the OME flame structures are well reproduced, while a couple of species and reaction pathways are seen to be less convincing, supplying a target for further model improvements.

Acknowledgments

First the authors want to thank Katharina Kohse-Höinghaus for offering the possibility to perform the MBMS flame measurements in her lab in Bielefeld at the turbulent times of the COVID pandemic. We are very grateful for her tremendous effort making this campaign possible in summer 2020. Her ongoing interest, countless valuable suggestions and fruitful discussions have not been less important for this work. NG, TB, JZ, PO and MK express an additional acknowledgement to Katharina Kohse-Höinghaus

for the possibility of taking over and moving the MBMS-flame system to DLR Stuttgart. HZ would like to express sincere gratitude to Katharina Kohse-Höinghaus for hosting him as a Humboldt research fellow in her lab.

The authors acknowledge support from the Deutsche Forschungsgemeinschaft (DFG) under contract KA3871/3-2 and KO4786/2-2. The research leading to these results has received funding from the European Community's Seventh Framework Program (FP7/2007-2013) under grant agreement no. 312284. Financial support is also acknowledged by the DLR project QSP Future Fuels. Patrick Hemberger also acknowledges support from the Swiss Federal Office of Energy (SFOE) under contract SI/501269-01. Hao Zhang is grateful for a fellowship of the Alexander von Humboldt Foundation. The experiments were performed at the VUV (X04DB) beamline of the Swiss Light Source (SLS) at Paul Scherrer Institute and at Bielefeld University. The authors gratefully thank Luka Debenjak, Patrick Ascher, Harald Waterbör and Marcel Frietsch for technical assistance as well as the members of the SLS flame team. Furthermore, all authors would like to thank Isabelle Graf for her support measuring flame temperatures.

References

[1] K. Kohse-Höinghaus, Combustion in the future: The importance of chemistry, Proc. Combust. Inst. 38(1) (2020) 1-56.

[2] N. Hansen, T.A. Cool, P.R. Westmoreland, K. Kohse-Höinghaus, Recent contributions of flame-sampling molecular-beam mass spectrometry to a fundamental understanding of combustion chemistry, Prog. Energy Combust. Sci. 35(2) (2009) 168-191.

[3] M. Schenk, L. Leon, K. Moshammer, P. Oßwald, T. Zeuch, L. Seidel, F. Mauss, K. Kohse-Höinghaus, Detailed mass spectrometric and modeling study of isomeric butene flames, Combust. Flame 160(3) (2013) 487-503.

[4] U. Struckmeier, P. Oßwald, T. Kasper, L. Böhling, M. Heusing, M. Köhler, A. Brockhinke, K. Kohse-Höinghaus, Sampling probe influences on temperature and species concentrations in molecular beam mass spectroscopic investigations of flat premixed low-pressure flames, Z. Phys. Chem. 223 (2009) 503-537.

[5] J. Burger, M. Siegert, E. Ströfer, H. Hasse, Poly(oxymethylene) dimethyl ethers as components of tailored diesel fuel: properties, synthesis and purification concepts, Fuel 89(11) (2010) 3315-3319.

[6] S. Peukert, P. Sela, D. Nativel, J. Herzler, M. Fikri, C. Schulz, Direct measurement of high-temperature rate constants of the thermal decomposition of dimethoxymethane, a shock tube and modeling study, J. Phys. Chem. A 122 (2018) 7559-7572.

[7] B. Li, Y. Li, H. Li, F. Liu, Z. Wang, J. Wang, Combustion and emission characteristics of diesel engine fueled with biodiesel/PODE blends, Appl. Energy 206 (2017) 425-431.

[8] W.A. Kopp, L.C. Kröger, M. Döntgen, S. Jacobs, U. Burke, H.J. Curran, K.A. Heufer, K. Leonhard, Detailed kinetic modeling of dimethoxymethane. Part I: Ab initio thermochemistry and kinetics predictions for key reactions, Combust. Flame 189 (2018) 433-442.

[9] L. Marrodán, F. Monge, Á. Millera, R. Bilbao, M. U., Alzueta, Dimethoxymethane oxidation in a flow reactor, Combust. Sci. Technol. 188 (2016) 719-729.

[10] F. Vermeire, H.-H. Carstensen, O. Herbinet, F. Battin-Leclerc, G. Marin, K.V. Geem, Experimental and modeling study of the pyrolysis and combustion of dimethoxymethane, Combust. Flame 190 (2018) 270-283.

[11] S. Jacobs, M. Döntgen, A.B.S. Alquaity, W.A. Kopp, L.C. Kröger, U. Burke, H. Pitsch, K. Leonhard, H.J. Curran, K.A. Heufer, Detailed kinetic modeling of dimethoxymethane. Part II: Experimental and theoretical study of the kinetics and reaction mechanism, Combust. Flame 205 (2019) 522-533.

[12] W. Sun, G. Wang, S. Li, R. Zhang, B. Yang, J. Yang, Y. Li, C.K. Westbrook, K. Chung, C.K. Law, Speciation and the laminar burning velocities of poly(oxymethylene) dimethyl ether 3 (POMDME3) flames: An experimental and modeling study, Proc. Combust. Inst. 36(1) (2017) 1269-1278.

[13] W. Sun, B. Yang, N. Hansen, K. Moshammer, The influence of dimethoxy methane (DMM)/dimethyl carbonate (DMC) addition on a premixed ethane/oxygen/argon flame, Proc. Combust. Inst. 36(1) (2017) 449-457.

[14] T. He, Z. Wang, X. You, H. Liu, Y. Wang, X. Li, X. He, A chemical kinetic mechanism for the low- and intermediate-temperature combustion of Polyoxymethylene Dimethyl Ether 3 (PODE3), Fuel 212 (2018) 223-226.

[15] J.M. Ngugi, S. Richter, M. Braun-Unkhoff, C. Naumann, M. Köhler, U. Riedel, A study on fundamental combustion properties of oxymethylene ether-2, OME2, Proceedings of ASME Turbo Expo 2021 Turbomachinery Technical Conference and Exposition, Virtual (2021).

[16] S. Eckart, L. Cai, C. Fritsche, F. vom Lehn, H. Pitsch, H. Krause, Laminar burning velocities, CO, and NOx emissions of premixed polyoxymethylene dimethyl ether flames, Fuel 293 (2021) 120321.

[17] S. Drost, R. Schießl, M. Werler, J. Sommerer, U. Maas, Ignition delay times of polyoxymethylene dimethyl ether fuels (OME2 and OME3) and air: Measurements in a rapid compression machine, Fuel 258 (2019) 116070.

[18] L. Cai, S. Jacobs, R. Langer, F.v. Lehn, K.A. Heufer, H. Pitsch, Auto-ignition of oxymethylene ethers (OME_n , n = 2–4) as promising synthetic e-fuels from renewable electricity: shock tube experiments and automatic mechanism generation, Fuel 264 (2020) 116711.

[19] S. Ren, Z. Wang, B. Li, H. Liu, J. Wang, Development of a reduced polyoxymethylene dimethyl ethers (PODEn) mechanism for engine applications, Fuel 238 (2019) 208-224.

[20] T. Kathrotia, P. Oßwald, C. Naumann, S. Richter, M. Köhler, Combustion kinetics of alternative jet fuels, Part-II: Reaction model for fuel surrogate, Fuel 302 (2021) 120736.

[21] P. Oßwald, J. Zinsmeister, T. Kathrotia, M. Alves-Fortunato, V. Burger, R.v.d. Westhuizen, C. Viljoen, K. Lehto, R. Sallinen, Kati Sandberg, M. Aigner, P.L. Clercq, M. Köhler, Combustion kinetics of alternative jet fuels, Part-I: Experimental flow reactor study, Fuel 302 (2021) 120735.

[22] T. Kathrotia, P. Oßwald, J. Zinsmeister, T. Methling, M. Köhler, Combustion kinetics of alternative jet fuels, Part-III: Fuel modeling and surrogate strategy, Fuel 302 (2021) 120737.

[23] D. Felsmann, A. Lucassen, J. Krüger, C. Hemken, L.-S. Tran, J. Pieper, G.A. Garcia, A. Brockhinke, L. Nahon, K. Kohse-Höinghaus, Progress in fixed-photon-energy time-efficient double imaging photoelectron/photoion coincidence measurements in quantitative flame analysis, Z. Phys. Chem. 230(8) (2016) 1067-1097.

[24] D. Felsmann, K. Moshammer, J. Krüger, A. Lackner, A. Brockhinke, T. Kasper, T. Bierkandt, E. Akyildiz, N. Hansen, A. Lucassen, P. Oßwald, M. Köhler, G.A. Garcia, L. Nahon, P. Hemberger, A. Bodi, T. Gerber, K. Kohse-Höinghaus, Electron ionization, photoionization and photoelectron/photoion coincidence spectroscopy in mass-spectrometric investigations of a low-pressure ethylene/oxygen flame, Proc. Combust. Inst. 35(1) (2015) 779-786.

[25] P. Oßwald, K. Kohse-Höinghaus, U. Struckmeier, T. Zeuch, L. Seidel, L. Leon, F. Mauss, Combustion chemistry of the butane isomers in premixed low-pressure flames, Z. Phys. Chem. 225(9-10) (2011) 1029-1054.

[26] L. Seidel, K. Moshammer, X. Wang, T. Zeuch, K. Kohse-Höinghaus, F. Mauss, Comprehensive kinetic modeling and experimental study of a fuel-rich, premixed n-heptane flame, Combust. Flame 162(5) (2015) 2045-2058.

[27] P. Oßwald, P. Hemberger, T. Bierkandt, E. Akyildiz, M. Köhler, A. Bodi, T. Gerber, T. Kasper, In situ flame chemistry tracing by imaging photoelectron photoion coincidence spectroscopy, Rev. Sci. Instrum. 85(2) (2014) 1-11.

[28] T. Bierkandt, P. Hemberger, P. Oßwald, D. Krüger, M. Köhler, T. Kasper, Flame structure of laminar premixed anisole flames investigated by photoionization mass spectrometry and photoelectron spectroscopy, Proc. Combust. Inst. 37 (2019) 1579-1588.

[29] D. Krüger, P. Oßwald, M. Köhler, P. Hemberger, T. Bierkandt, T. Kasper, The fate of the OH radical in molecular beam sampling experiments, Proc. Combust. Inst. 37 (2019) 1563-1570.

[30] C. Morley, GasEQ - A Chemical Equilibrium Program, http://www.gaseq.co.uk/.

[31] Bronkhorst. Theory and advantages of 'CEM' Vapour Control; Available from: https://www.bronkhorst.com/en-gb/service-support-en/technologies/theory-and-advantages-of-cem-vapour-control/. [Accessed 11/01/2022 2021].

[32] H. Zhang, D. Kaczmarek, C. Rudolph, S. Schmitt, N. Gaiser, P. Oßwald, T. Bierkandt, T. Kasper, B. Atakan, K. Kohse-Höinghaus, Dimethyl ether (DME) and dimethoxymethane (DMM) as reaction enhancers for methane: combining flame experiments with model-assisted exploration of a polygeneration process, revised manuscript submitted to Combust. Flame (2021).

[33] P. Hemberger, A. Bodi, T. Bierkandt, M. Köhler, D. Kaczmarek, T. Kasper, Photoelectron photoion coincidence spectroscopy provides mechanistic insights in fuel synthesis and conversion, Energy Fuels 35 (2021) 16265-16302.

[34] B. Yang, J. Wang, T.A. Cool, N. Hansen, S. Skeen, D.L. Osborn, Absolute photoionization cross-sections of some combustion intermediates, Int. J. Mass Spectrom. 309 (2012) 118-128.

[35] T. Bierkandt, P. Hemberger, P. Oßwald, M. Köhler, E. Akyildiz, A. Bodi, T. Gerber, T. Kasper, Distinguishing reactive isomers in premixed laminar low-pressure flames by using PEPICO spectroscopy, Proceedings of the European Combustion Meeting, 7th European Combustion Meeting (ECM), Budapest, Hungary (30.03.-02.04.2015).

[36] T. Bierkandt, P. Hemberger, P. Oßwald, M. Köhler, T. Kasper, Insights in m-xylene decomposition under fuel-rich conditions by imaging photoelectron photoion coincidence spectroscopy, Proc. Combust. Inst. 36(1) (2017) 1223-1232.

[37] J.C. Biordi, Molecular beam mass spectrometry for studying the fundamental chemistry of flames, Prog. Energy Combust. Sci. 3(3) (1977) 151-173.

[38] A. Schocker, M. Uetake, N. Kanno, M. Koshi, K. Tonokura, Kinetics and rate constants of the reaction CH2OH + O2 → CH2O + HO2 in the temperature range of 236−600 K, J. Phys. Chem. 1111 (2006) 6622-6627.

[39] D. Krüger, P. Oßwald, M. Köhler, P. Hemberger, T. Bierkandt, Y. Karakaya, T. Kasper, Hydrogen abstraction ratios: A systematic iPEPICO spectroscopic investigation in laminar flames, Combust. Flame 191 (2018) 343-352.

[40] T. Bierkandt, P. Oßwald, N. Gaiser, D. Krüger, M. Köhler, M. Hoener, S. Shaqiri, D. Kaczmarek, Y. Karakaya, P. Hemberger, T. Kasper, Observation of low-temperature chemistry products in laminar premixed low-pressure flames by molecular-beam mass spectrometry, Int. J. Chem. Kinet. 53 (2021) 1063-1081.

[41] X. Zhang, Y. Zhang, T. Li, Y. Li, J. Zou, P. Dagaut, J. Yang, W. Li, M. Zeng, H. Jin, W. Yuan, F. Qi, Low-temperature chemistry triggered by probe cooling in a low-pressure premixed flame, Combust. Flame 204 (2019) 260-267.

[42] A.T. Hartlieb, B. Atakan, K. Kohse-Höinghaus, Effects of a sampling quartz nozzle on the flame structure of a fuel-rich low-pressure propene flame, Combust. Flame 121 (2000) 610-624.

[43] L. Deng, A. Kempf, O. Hasemann, O.P. Korobeinichev, I. Wlokas, Investigation of the sampling nozzle effect on laminar flat flames, Combust. Flame 162(5) (2015) 1737-1747.

[44] Y. Karakaya, J. Sellmann, I. Wlokas, T. Kasper, Influence of the sampling probe on flame temperature, species, residence times and on the interpretation of ion signals of methane/oxygen flames in molecular beam mass spectrometry measurements, Combust. Flame 229 (2021) 111388.

[45] A. Lucassen, N. Labbe, P.R. Westmoreland, K. Kohse-Höinghaus, Combustion chemistry and fuel-nitrogen conversion in a laminar premixed flame of morpholine as a model biofuel, Combust. Flame 158(9) (2011) 1647-1666.

[46] N. Bahlawane, U. Struckmeier, T. Kasper, P. Oßwald, Noncatalytic thermocouple coatings produced with chemical vapor deposition for flame temperature measurements, Rev. Sci. Instrum. 78(1) (2007) 013905.

[47] I. Graf, Personal Communication (2020).

[48] X. Yang, D. Felsmann, N. Kurimoto, J. Krüger, T. Wada, T. Tan, E.A. Carter, K. Kohse-Höinghaus, Y. Ju, Kinetic studies of methyl acetate pyrolysis and oxidation in a flow reactor and a low-pressure flat flame using molecular-beam mass spectrometry, Proc. Combust. Inst. 35(1) (2015) 491-498.

[49] D.G. Goodwin, R.L. Speth, H.K. Moffat, B.W. Weber, Cantera: An object-oriented software toolkit for chemical kinetics, thermodynamics, and transport processes, Version 2.5.1 http://www.cantera.org (2021).

[50] Chemical Workbench, Version 4.1.19528 http://www.kintechlab.com/ (2017).

[51] K.P. Shrestha, S. Eckart, A.M. Elbaz, B.R. Giri, C. Fritsche, L. Seidel, W.L. Roberts, H. Krause, F. Mauss, A comprehensive kinetic model for dimethyl ether and dimethoxymethane oxidation and NO interaction utilizing experimental laminar flame speed measurements at elevated pressure and temperature, Combust. Flame 218 (2020) 57-74.

[52] S. Richter, T. Kathrotia, M. Braun-Unkhoff, C. Naumann, M. Köhler, Influence of oxymethylene ethers (OMEn) in mixtures with a Diesel surrogate, submitted to Energies 14 (2021).

[53] J.M. Ngugi, S. Richter, M. Braun-Unkhoff, C. Naumann, U. Riedel, An investigation of fundamental combustion properties of the oxygenated fuels DME and OME1, Proceedings of ASME Turbo Expo 2020: Turbomachinery Technical Conference and Exposition, Volume 3: Ceramics; Coal, Biomass, Hydrogen, and Alternative Fuels, Virtual, Online.

[54] B. Niu, M. Jia, Y. Chang, H. Duan, X. Dong, P. Wang, Construction of reduced oxidation mechanisms of polyoxymethylene dimethyl ethers (PODE1–6) with consistent structure using decoupling methodology and reaction rate rule, Combust. Flame 232 (2021).

[55] N. Gaiser, T. Bierkandt, P. Oßwald, J. Zinsmeister, T. Kathrotia, S. Shaqiri, P. Hemberger, T. Kasper, M. Aigner, M. Köhler, Oxidation of oxymethylene ether (OME0-5): An experimental systematic study by mass spectrometry and photoelectron photoion coincidence spectroscopy, Fuel, in press (2021) 122650

[56] Z. Wang, H. Liu, X. Ma, J. Wang, S. Shuai, R. D.Reitz, Homogeneous charge compression ignition (HCCI) combustion of polyoxymethylene dimethyl ethers (PODE), Fuel 183 (2016) 206-213.

[57] K. Kohse-Höinghaus, P. Oßwald, T.A. Cool, T. Kasper, N. Hansen, F. Qi, C.K. Westbrook, P.R. Westmoreland, Biofuel combustion chemistry: from ethanol to biodiesel, Angew. Chem. Int. Ed. Engl. 49(21) (2010) 3572-3597.

[58] J. Wang, M. Chaos, B. Yang, T.A. Cool, F.L. Dryer, T. Kasper, N. Hansen, P. Oßwald, K. Kohse-Höinghaus, P.R. Westmoreland, Composition of reaction intermediates for stoichiometric and fuel-

rich dimethyl ether flames: flame-sampling mass spectrometry and modeling studies, Phys. Chem. Chem. Phys. 11(9) (2009) 1328-1339.

[59] C.A. Taatjes, N. Hansen, A. McIlroy, J.A. Miller, J.P. Senosiain, S.J. Klippenstein, F. Qi, L. Sheng, Y. Zhang, T.A. Cool, J. Wang, P.R. Westmoreland, M.E. Law, T. Kasper, K. Kohse-Höinghaus, Enols are common intermediates in hydrocarbon oxidation, Science 308(5730) (2005) 1887-1889.

[60] T. Kasper, A. Lucassen, A.W. Jasper, W. Li, P.R. Westmoreland, K. Kohse-Höinghaus, B. Yang, J. Wang, T.A. Cool, N. Hansen, Identification of tetrahydrofuran reaction pathways in premixed flames, Z. Phys. Chem. 225(11-12) (2011) 1237-1270.

[61] T.A. Cool, A. McIlroy, F. Qi, P.R. Westmoreland, L. Poisson, D.S. Peterka, M. Ahmed, Photoionization mass spectrometer for studies of flame chemistry with a synchrotron light source, Rev. Sci. Instrum. 76(9) (2005) 1-7.

[62] T.A. Cool, K. Nakajima, T.A. Mostefaoui, Selective detection of isomers with photoionization mass spectrometry for studies of hydrocarbon flame chemistry, J. Chem. Phys. 119(16) (2003) 8356.

[63] T.A. Cool, J. Wang, K. Nakajima, C.A. Taatjes, A. Mcllroy, Photoionization cross sections for reaction intermediates in hydrocarbon combustion, Int. J. Mass Spectrom. 247(1-3) (2005) 18-27.

[64] R.D. Bach, J.L. Andres, A.L. Owensby, H.B. Schlegel, J.J.W. McDouall, Electronic structure and reactivity of dioxirane and carbonyl oxide, J. Am. Chem. Soc. 114(18) (1992) 7207-7217.

[65] M.T. Nguyen, T.L. Nguyen, V.T. Ngan, H.M.T. Nguyen, Heats of formation of the Criegee formaldehyde oxide and dioxirane, Chem. Phys. Lett. 448(4-6) (2007) 183-189.

[66] O. Welz, J.D. Savee, D.L. Osborn, S.S. Vasu, C.J. Percival, D.E. Shallcross, C.A. Taatjes, Direct kinetic measurements of criegee intermediate (CH2OO) formed by reaction of CH2I with O2, Science 335 (2012) 204-208.

[67] D.V. Chicharro, S.M. Poullain, L. Bañares, H.R. Hrodmarsson, G.A. García, J.-C. Loison, Threshold photoelectron spectrum of the CH2OO criegee intermediate, Phys. Chem. Chem. Phys. (24) (2019) 12763-12766

[68] K. Kimura, S. Katsumata, Y. Achiba, T. Yamazaki, S. Iwata. Handbook of HeI photoelectron spectra of fundamental organic molecules. Japan: Japan Scientific Society Press; 1981.

[69] Y. Nunes, G. Martins, N.J. Mason, D. Duflot, S.V. Hoffmann, J. Delwiche, M.-J. Hubin-Franskin, P. Limão-Vieira, Electronic state spectroscopy of methyl formate probed by high resolution VUV photoabsorption, He(I) photoelectron spectroscopy and ab initio calculations, Phys. Chem. Chem. Phys. (48) (2010) 15734-15743

[70] C.A. Taatjes, O. Welz, A.J. Eskola, J.D. Savee, A.M. Scheer, D.E. Shallcross, B. Rotavera, E.P.F. Lee, J.M. Dyke, D.K.W. Mok, D.L. Osborn, C.J. Percival, Direct measurements of conformer-dependent reactivity o the criegee intermediate CH3CHOO, Science 340 (2013) 177-182.

[71] T. Yu, X. Wu, X. Zhou, A. Bodi, P. Hemberger, Hydrogen migration as a potential driving force in the thermal decomposition of dimethoxymethane: New insights from pyrolysis imaging photoelectron photoion coincidence spectroscopy and computations, Combust. Flame 222 (2020) 123-132.

[72] T.A. Cool, J. Wang, N. Hansen, P.R. Westmoreland, F.L. Dryer, Z. Zhao, A. Kazakov, T. Kasper, K. Kohse-Höinghaus, Photoionization mass spectrometry and modelingstudies of the chemistry of fuel-richdimethyl ether flames, Proc. Combust. Inst. 31 (2007) 285-293.

[73] K. Yasunaga, M. Simmie, H.J. Curran, T. Koike, O. Takahashi, Y. Kuraguchi, Y. Hidaka, Detailed chemical kinetic mechanisms of ethyl methyl, methyl tert-butyl and ethyl tert-butyl ethers: The importance of uni-molecular elimination reactions, Combust. Flame 158 (2011) 1032-1036.

[74] O. Welz, M.P. Burke, I.O. Antonov, C.F. Goldsmith, J.D. Savee, D.L. Osborn, C.A. Taatjes, S.J. Klippenstein, L. Sheps, New insights into low-temperature oxidation of propane from synchrotron photoionization mass spectrometry and multiscale informatics modeling, J. Phys. Chem. A 119(28) (2015) 7116-7129.